PAPER

Check for updates

Dipole orientation-induced interfacial energy level alignment difference in 2D perovskite passivated 3D perovskite by *in situ* investigation†

Ruifeng Zheng,‡ Jielei Li,‡ Shengwen Li,* Bingchen He and Shi Chen [ID] *

Interface passivation has been widely used in perovskite solar cell studies with multiple beneficial effects. Among them, energy level alignment is frequently mentioned but is mostly studied by *ex situ* measurement, which is unable to reveal subtle changes at the interface. In this study, we *in situ* investigated the interfacial energy alignment of $MAPbI_3$ passivated by two ammonium salts with long alkyl chains (butylammonium iodide and butane-1,4-diammonium iodide, BAI and BDAI). Both molecules formed a 0.11 eV interface dipole, but in opposite directions. The BAI deposition created an additional downward band bending on the BAI side, making it ideal for electron extraction. The BDAI deposition created an additional 0.12 eV valence band maximum (VBM) drop, imposing a barrier for hole transfer. Such non-optimum alignment could partially explain the lower device performance with BDAI passivation. Our results highlight the importance of *in situ* studies and reveal unseen details in the electronic structure at the passivation interface.

1   Introduction

Perovskite solar cells (PSCs) have attracted great attention in next-generation photovoltaics due to the excellent optoelectronic properties of metal halide perovskites, such as broad and strong light absorption,[1] long carrier lifetime, small exciton binding energy,[2] benign defect physics,[3] and excellent solution processability.[4] To date, the power conversion efficiency (PCE) of single-junction PSCs has been improved to 27.0%,[5] which is comparable to that of commercially available silicon cells. In the development of PSCs, three strategies have been extensively explored: composition adjustment, crystallization optimization, and interfacial engineering.[6,7]

Interfacial passivation aims to reduce interfacial defects and protect the perovskite from decomposition by internal and external stresses. The popularity of this strategy has been evidenced by more than 3000 papers published in the past decade. It is not surprising that a tremendous amount of passivation agents have been applied to the perovskite interfaces, such as inorganic salts, organic molecules, and polymers.[8–10] Among all passivation agents, organic ammonium cations (2D cations) are particularly attractive because they could form thin 2D perovskite layers on 3D perovskites epitaxially. The 2D perovskite also has better compatibility with the 3D perovskite in terms of

composition and crystallinity compared to heterogeneous agents. Long organic ammonium salts could effectively passivate surface cation/anion defects and repel water incursion. Various organic ammonium salts are used for interfacial passivation. These salts include monoammonium salts such as ethylammonium iodide (EAI), butylammonium iodide (BAI), octylammonium iodide (OAI), pentafluorophenylethylammonium iodide (FEAI), phenethylammonium iodide (PEAI) *etc.* and diammonium salts such as ethane diammonium iodide (EDAI), butane diammonium iodide (BDAI), dimethylpropane diammonium iodide (DMPDAI) *etc.*[11–15] As more and more ammonium salts appear effective in passivation, it is scientifically important to find out which salt is more effective than the others. The guidelines from such studies can help to find better salts for passivation and explain the passivation effect of different salts. A few guidelines are frequently suggested in the literature, such as interfacial defect passivation, Pb^0 suppression, better crystallinity, and improved energy level alignment.[16,17] However, these discussions heavily rely on device performance. The fundamental investigation into each guideline is still limited.

One such puzzle is to find which category of ammonium salts is more effective: monoammonium salts or diammonium salts. Monoammonium salts contain only one ammonium group, which requires weaker dipole–dipole interactions (hydrogen bonds, van der Waals interactions) to link different domains, while diammonium salts with two ammonium groups could link two perovskite domains directly. In principle, diammonium salts should show better performance in passivated devices because they could bind different domains strongly.

Institute of Applied Physics and Materials Engineering, University of Macau, Macau SAR 999078, P. R. China. E-mail: shengwenli@um.edu.mo; shichen@um.edu.mo

‡ These authors contributed equally.

However, from the literature, we clearly see that mono-ammonium salts are more widely used and generally show better device performance than their diammonium counterparts. For example, butane ammonium iodide (BAI) and butane diammonium iodide (BDAI) are two molecules that share the same organic backbones, differing only in the number of ammonium groups. The reported studies show that the BAI passivated device can achieve performance of about 23% or above, while the BDAI passivated device only shows performance of about 20 to 22%. Another example is phenethylammonium iodide (PEAI) and its counterparts: *p*-xylylenediammonium iodide (XDAI) and *p*-phenylenediaminium iodide (PDAI). Both diammonium salts appear less effective than PEAI in passivation.[18,19] Such differences may originate from various reasons: effectiveness of defect passivation, impact on crystallization orientation, film uniformity, and energy level alignment. However, the first three causes are usually carefully examined by various structural, optical, and compositional methods, leaving the last cause rarely investigated. Due to the presence of two ammonium groups in the diammonium molecules, the dipole moment inside these 2D cations points toward each other, creating an energy barrier for both electrons and holes. Also, more ammonium groups could induce stronger charge transfer and cause more obvious band bending. Therefore, a thorough investigation of this interface by *in situ* methods should be carried out to reveal the different energy level alignments of these two types of molecules at the perovskite interface.

In this paper, we studied two ammonium salts, BAI and BDAI, as the model system by *in situ* deposition and measurement to reveal the difference in electronic structures at the interface. Our study revealed different interfacial electronic structures for the two salts. First, we observed that the interfacial dipole generated by the two molecules pointed in the opposite direction. An outward dipole of 0.11 eV is found with BAI molecule deposition, while a dipole of the same magnitude points inward with BDAI deposition. Second, both molecules induced band bending on the molecular side with similar magnitudes (0.24 eV and 0.29 eV for BAI and BDAI, respectively). However, BDAI shows stronger charge transfer and induces an obvious band bending in the
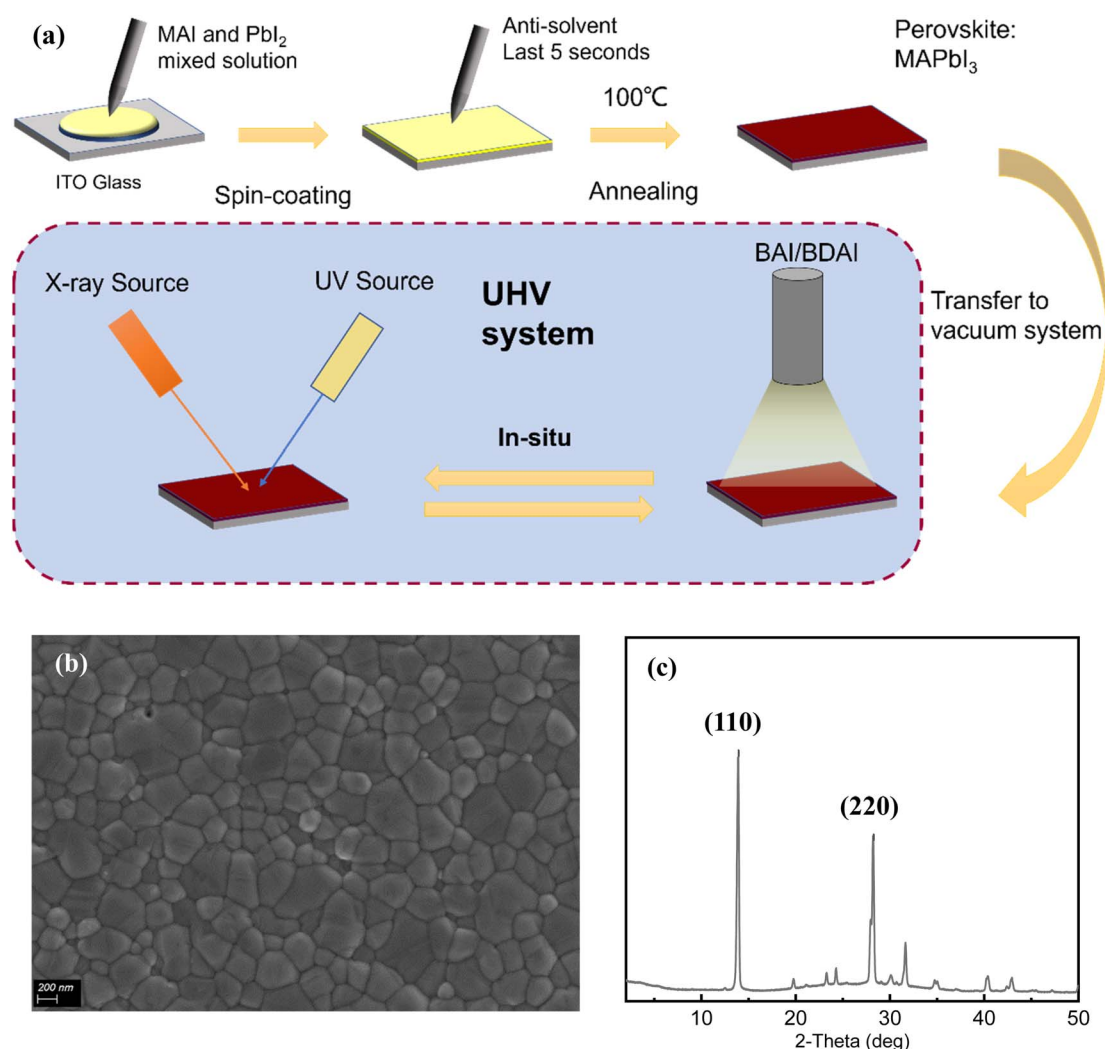

Fig. 1 (a) Schematic diagram of the experimental process; (b) SEM and (c) XRD images of substrate perovskite (MAPbI$_3$).

perovskite, while this bending is negligible in contact with the BAI molecule. Third, the BDAI passivated surface shows a band offset of 0.12 eV at the interface, while the BAI passivated surface shows no band offset. From our study, it can be seen that BDAI could cause a more complex interfacial electronic structure, which could either restrain electron transfer (*via* interfacial dipole) or hole transfer (*via* band offset). Such complexity at the interface could help us understand why diammonium salts are less effective than monoammonium salts from an energetic point of view. Our study also suggests that the diammonium salts with better electron/hole transfer selectivity could reduce the interfacial loss in perovskite passivation.

2   Results and discussion

Vacuum evaporation was calibrated on ITO substrates to determine suitable growth temperatures and rates. The chemical structures of the molecules are shown in Fig. S1.† After evaporation of BAI, two C 1s peaks at 284.88 eV and 286.47 eV were observed, corresponding to the C–C bond and the C–N bond, respectively (Fig. S2†). The area ratio of the two peaks was 2.95 : 1, which is consistent with the C/N ratio in BAI. At the same time, an iodine peak was observed at 619.75 eV. From the XPS measurement, BAI can be vapor-deposited on the ITO glass without noticeable decomposition. The vacuum deposition of BDAI was also measured by XPS, confirming the integrity of the

molecules by elemental ratio (Fig. S3 and Table S2†). Nevertheless, both molecules exhibited slight iodine enrichment on the surface, which may suggest partial iodine accumulation on the surface.

To prepare a pristine perovskite surface for *in situ* measurement, a $MAPbI_3$ film was prepared by a standard spin coating and annealing procedure in a glovebox. The preparation details can be found in the experimental section. The substrate was transferred in an air-tight container to the XPS system without exposure to air. The quality of the prepared perovskite film was checked by scanning electron microscopy (SEM) and XRD (Fig. 1). The SEM images showed an intact film with an average grain size of about 300 nm without obvious surface defects (Fig. 1a). The results of XRD are shown in Fig. 1b, showing obvious (110) and (220) characteristic peaks at 14.1° and 28.2°, confirming the good crystallinity without any impurity phases such as PbI_2.

The SEM images of the pristine perovskite and perovskites after the evaporation process are shown in Fig. S4.† The extra clusters and increased roughness prove the successful deposition of the molecules. The *in situ* evaporation of BAI molecules on perovskite ($MAPbI_3$) was cross-checked by attenuation of XPS peaks and quartz crystal microbalance (QCM) measurements in Fig. 2. With continuous BAI deposition, the peaks of Pb 4f and I 3d decreased constantly. In the C 1s peak, the change is slightly complicated. In pristine perovskite, two carbon peaks are
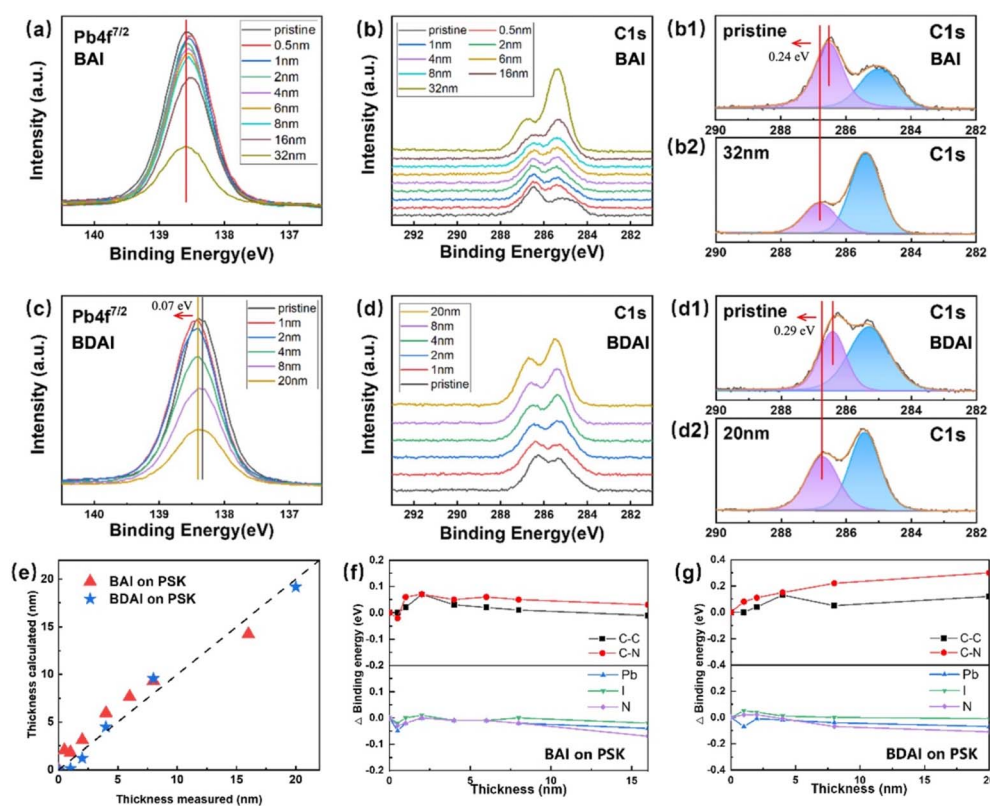

Fig. 2 (a and b) XPS images of BAI grown on perovskite substrates; (c and d) XPS images of BDAI grown on perovskite substrates; (e) comparison of film thickness calculated by attenuation of Pb 4f peaks and thickness measured using a quartz crystal microbalance (QCM); (f and g) the shift of binding energy with thickness.

observed at 284.91 eV and 286.51 eV due to the adventitious carbon and C–N bonds in MA cations. After deposition of BAI molecules, a new C 1s peak appeared around 285.4 eV, from C–C bonds in the BAI molecule. The adventitious C 1s peak gradually attenuated, while the peak at 286.5 eV first decreased and then increased. The attenuation of the first peak is due to the coverage of BAI molecules on top of the MAPbI$_3$ surface. The enhancement of the second peak is due to C–N bonds in BAI itself. The intensity change of the C–N peak is consistent with the change in N 1s spectra. There is no peak shift in the Pb 4f peak and other elements, indicating no band bending on the perovskite side. The carbon and nitrogen peak positions are both shifted by 0.24 eV to the higher binding energy side, which could be understood due to an upward band bending on the BAI side. A similar peak intensity change is also observed with BDAI deposition, confirming a similar growth mode. In BDAI deposition, we observed an additional shift of the Pb 4f and I 3d peaks to the higher binding energy side by 0.07 eV. This small shift reveals that the interaction of BDAI with perovskite is stronger, inducing additional band bending on the perovskite side. As a result, the shift on the BDAI side is also slightly larger, reaching 0.29 eV. Fig. 2e shows the comparison of the calculated film thickness by XPS attenuation with the QCM value. The fitting line follows closely along 45°, suggesting that the growth of the two molecules follows the Frank–van der Merwe growth model (commonly known as the layer-by-layer growth model).

The work function (WF) and valence band maximum (VBM) of the film were measured by UPS (Ultraviolet Photoelectron Spectroscopy) (Fig. 3). After deposition of the first 0.5 nm of BAI,

the WF decreased by 0.11 eV with no obvious change in the valence band. Such a change indicates that a surface dipole of about 0.11 eV pointing toward BAI is formed. As the BAI film thickness increases, the WF and the VBM change continuously. The WF gradually reduces to 3.9 eV after deposition up to 32 nm. The VBM shows a constant decrease from 1.64 eV to 1.89 eV as the BAI thickness increases. The consistent shifts of WF and VBM suggest a 0.25 eV upward band bending at the interface. The deposition of BDAI shows a different change in WF and VBM. For WF, the value first increased to 4.1 eV and then decreased to 3.8 eV in subsequent deposition. The initial VBM is 1.64 eV. After 1 nm of BDAI deposition, the VBM drops with a magnitude of 0.12 eV. In subsequent growth, the VBM further dropped to 2.05 eV. From these data, the BDAI deposition also generates an upward band bending but with a larger magnitude of about 0.29 eV, while BAI only induces an upward band bending of 0.25 eV. The large band bending is probably related to the higher density of ammonium groups of BDAI molecules, which induces stronger charge transfer at the interface. In addition, the deposition of BDAI also induces an opposite dipole at the interface, with a similar magnitude to that of BAI (0.11 eV) but pointing toward the perovskite layer. The opposite interfacial dipole directions of BAI and BDAI suggest that the molecular dipole direction can modify the interfacial electrical field direction. Last, the BDAI deposition also causes a VBM shift of 0.12 eV, suggesting a band offset at the interface. Such an offset could have a negative impact on the hole extraction.
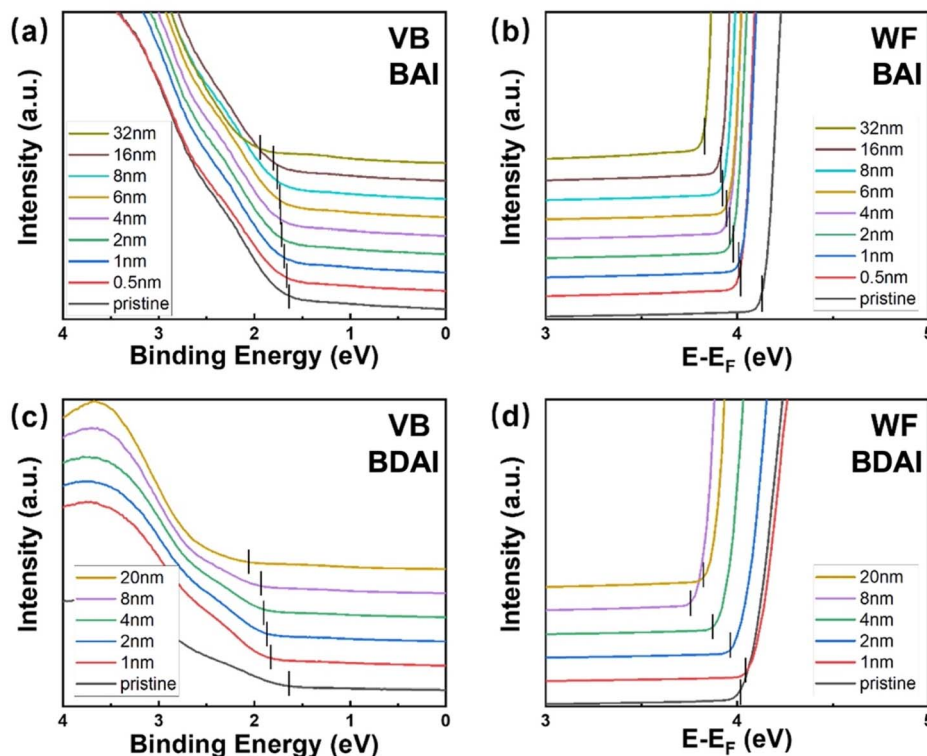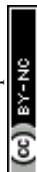

Fig. 3 UPS spectra of the interface of (a and b) PSK/BAI and (c and d) PSK/BDAI.
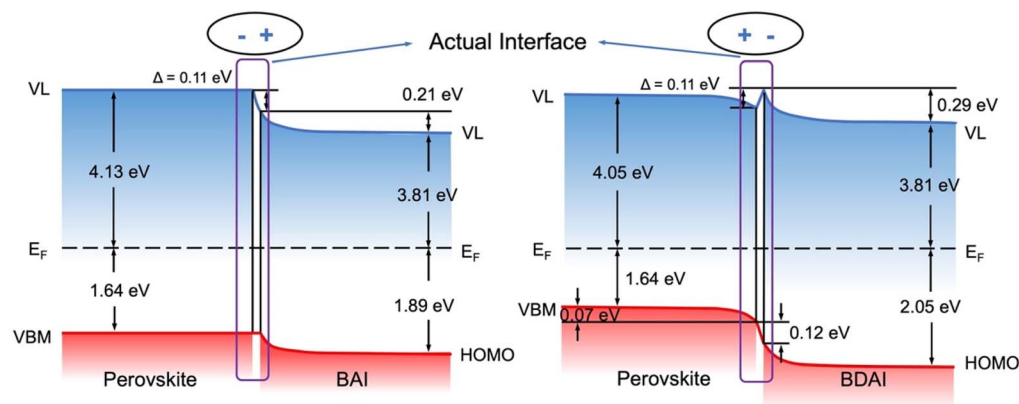
Fig. 4 Energy level diagram of the interface between perovskite and BAI/BDAI.

The interfacial energy structure is constructed based on the above data in Fig. 4. The band gap of BAI and BDAI is measured by UV-vis measurement (Fig. S6†). Both molecules are found to have the same band gap at 4.03 eV, suggesting that the LUMO of both molecules is the same. Furthermore, the VBM changes at the interface can be inferred for the conduction band too. Since in interfacial passivation, 2D perovskite layers should be very thin, the band structure in the vicinity of the interface is of particular interest. The direction of the interfacial dipole and band bending of BAI suggest that it is more suitable for electron transfer, though the magnitude of the dipole layer may only impose a finite impact on device performance. For BDAI, the dipole direction is reversed. Therefore, the hole transfer is encouraged rather than deterred. Nevertheless, the VBM band offset and band bending in perovskites still impose a small

barrier for hole transfer. Since the magnitude of the barrier is limited (0.12 eV), the BDAI passivation could still allow efficient hole transfer. As evidence, we observed that most of the highly efficient BDAI passivation studies use an inverted cell architecture. The non-optimum energetics of the BDAI/perovskite interface could be one reason for their inferior device performance (Fig. 5). The detailed information of the devices in Fig. 5 is shown in Table S7.† The V_{oc} and the fill factor of BDAI passivated devices are statistically lower than those of their BAI counterparts. However, when the 2D passivation layer is much thicker, the band bending at the passivation layer cannot be omitted, and the strong band bending may appear as a stronger obstacle to the hole transfer. Therefore, the 2D perovskite passivation should be kept thin from an energetic point of view.
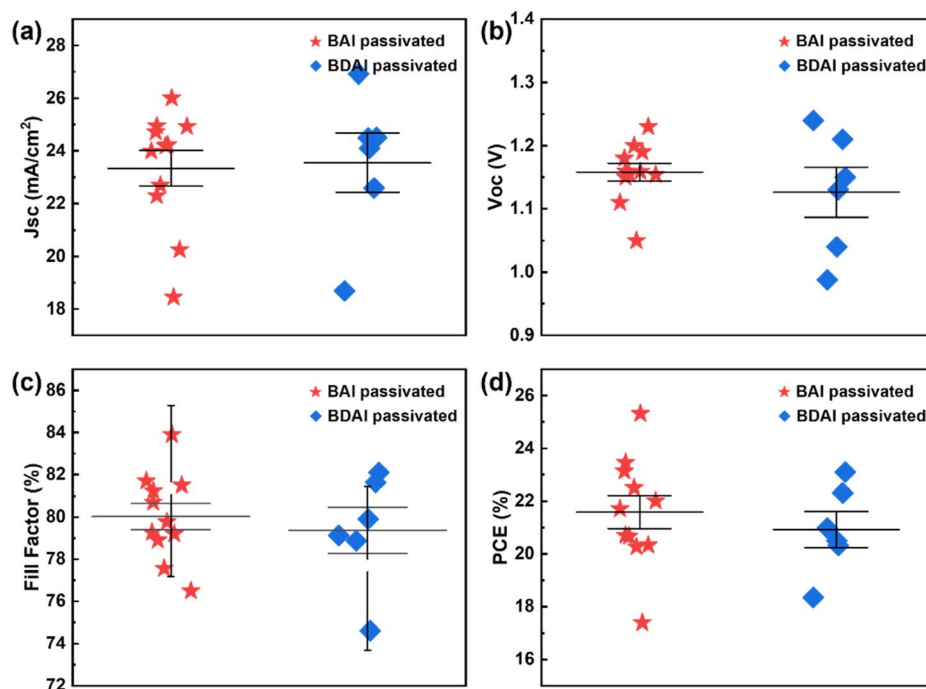

Fig. 5 Distribution of V_{OC}, J_{SC}, FF, and PCE in solar cells passivated with perovskite using BAI and BDAI in recent years.[6,12,14,20–32]

3 Conclusion

We used an *in situ* vacuum evaporation method to study the energy level structure of the interface between BAI and BDAI molecules and the perovskite layer. The two molecules induce very different interfacial energy structures. The BAI deposition only creates a simpler case with a 0.11 eV outward interfacial dipole with 0.25 eV band bending at the BAI layer only. The BDAI deposition causes multiple changes at the interface. Due to stronger interaction with perovskite, the perovskite layer also possesses a downward band bending of about 0.07 eV. The interfacial dipole created by BDAI deposition has the same magnitude as that of BAI (0.11 eV) but in the inward direction. BDAI also creates a VBM offset of about 0.05 eV, followed by 0.29 eV band bending. From our measurement, we find that when the passivation layer is thin, BAI is more suitable for electron transfer, while the interfacial structure of BDAI passivation prefers hole transfer due to its interfacial dipole, though the band offset of VBM may weaken this effect. In comparison, BDAI is more suitable for hole extraction. Our results partially explain the performance difference between BAI and BDAI passivation. We believe that more studies on interfacial energy level alignment through 2D passivation could help to identify better passivation agents for PSCs.

4 Experimental

4.1 Materials

All chemicals were purchased and used directly without further purification. PbI_2 (purity > 99.99%) and methylammonium iodide (MAI, purity ≥ 99.5%) were purchased from Xi'an Polymer Light Technology (China). Anhydrous dimethyl sulfoxide (DMSO, 99.9%), *n*-butylammonium iodide (BAI, purity ≥ 98%), and butane-1,4-diammonium iodide (BDAI, purity ≥ 98%) were obtained from Sigma-Aldrich (USA). Indium tin oxide glasses were bought from Yingkou Youxuan Commercial & Trading Co., Ltd (Yingkou, Liaoning, China).

4.2 Perovskite fabrication

4.2.1 Preparation of perovskite. 127.2 mg MAI and 368.8 mg PbI_2 were dissolved in 700 μL GBL and 300 μL DMSO, and the solution was stirred overnight. The mixed solution was spin-coated on the ITO substrate at 1500 rpm for 15 s and at 4000 rpm for 40 s, and the anti-solvent toluene was added dropwise in the last 15 s. Finally, it was annealed at 100 °C for 20 minutes to obtain $MAPbI_3$.

4.2.2 Evaporation of the perovskite surface modification layer. The BAI powder was placed in an evaporation source, heated to 50 °C for degassing for several hours, and then started to vaporize it onto the $MAPbI_3$ substrate at a temperature of 60 °C. The growth rate was determined using a film thickness meter during the evaporation process. Finally, a high-purity BAI modified layer was obtained. The evaporation method of BDAI was the same as that of BAI.

4.3 Characterization

The SEM images were captured using a Sigma field emission scanning electron microscope (Zeiss, Germany) at an accelerating voltage of 3 kV. The XRD patterns were measured using a Rigaku (RINT-2500) X-ray diffractometer with Cu Kα (λ = 1.5418 Å) radiation. X-ray photoelectron spectroscopy (XPS) and ultraviolet photoelectron spectroscopy (UPS) were performed on a Thermo Scientific ESCALAB Xi$^+$ to characterize the elemental composition and energy levels of the film.

Data availability

The data supporting this article have been included as part of the ESI.†

Conflicts of interest

The authors declare no conflict of interest.

Acknowledgements

References

1 S. De Wolf, *et al.*, Organometallic Halide Perovskites: Sharp Optical Absorption Edge and Its Relation to Photovoltaic Performance, *J. Phys. Chem. Lett.*, 2014, **5**(6), 1035–1039.

2 A. Miyata, *et al.*, Direct measurement of the exciton binding energy and effective masses for charge carriers in organic–inorganic tri-halide perovskites, *Nat. Phys.*, 2015, **11**(7), 582–587.

3 K. X. Steirer, *et al.*, Defect Tolerance in Methylammonium Lead Triiodide Perovskite, *ACS Energy Lett.*, 2016, **1**(2), 360–366.

4 J. Burschka, *et al.*, Sequential deposition as a route to high-performance perovskite-sensitized solar cells, *Nature*, 2013, **499**(7458), 316–319.

5 National Renewable Energy Laboratory (NREL), Research-Cell Efficiencies, 2022, Available from: **https://www.nrel.gov/pv/cell-efficiency.html**.

6 J. Wang, *et al.*, Ambient air processed highly oriented perovskite solar cells with efficiency exceeding 23% *via* amorphous intermediate, *Chem. Eng. J.*, 2022, **446**, 136968.

7 C. Gong, *et al.*, Functional-Group-Induced Single Quantum Well Dion–Jacobson 2D Perovskite for Efficient and Stable Inverted Perovskite Solar Cells, *Adv. Mater.*, 2024, **36**(8), 2307422.

8 A. Bhardwaj, *et al.*, In situ click chemistry generation of cyclooxygenase-2 inhibitors, *Nat. Commun.*, 2017, **8**(1), 1.

9 T. Zhao, *et al.*, Defect Passivation of Organic–Inorganic Hybrid Perovskites by Diammonium Iodide toward High-

Performance Photovoltaic Devices, *ACS Energy Lett.*, 2016, **1**(4), 757–763.

10 Y. Lin, *et al.*, Matching Charge Extraction Contact for Wide-Bandgap Perovskite Solar Cells, *Adv. Mater.*, 2017, **29**(26), 1700607.

11 X. Ye, *et al.*, Alkyl ammonium salt with different chain length for high-efficiency and good-stability 2D/3D hybrid perovskite solar cells, *Org. Electron.*, 2022, **106**, 106542.

12 S. Liu, *et al.*, Effective Passivation with Size-Matched Alkyldiammonium Iodide for High-Performance Inverted Perovskite Solar Cells, *Adv. Funct. Mater.*, 2022, **32**(38), 2205009.

13 N. Li, *et al.*, Mixed Cation FAxPEA1–xPbI3 with Enhanced Phase and Ambient Stability toward High-Performance Perovskite Solar Cells, *Adv. Energy Mater.*, 2017, **7**(1), 1601307.

14 H. W. Chang, *et al.*, Enhancing perovskite solar cell efficiency and stability through the incorporation of BDAI2 and DMPDAI2, *Energy Adv.*, 2024, **3**(3), 552–557.

15 X. Jiang, *et al.*, Direct Surface Passivation of Perovskite Film by 4-Fluorophenethylammonium Iodide toward Stable and Efficient Perovskite Solar Cells, *ACS Appl. Mater. Interfaces*, 2021, **13**(2), 2558–2565.

16 N. Chen, *et al.*, Universal band alignment rule for perovskite/organic heterojunction interfaces, *ACS Energy Lett.*, 2023, **8**(3), 1313–1321.

17 H. W. Chang, *et al.*, Enhancing perovskite solar cell efficiency and stability through the incorporation of BDAI 2 and DMPDAI 2, *Energy Adv.*, 2024, **3**(3), 552–557.

18 P. Zardari, A. Rostami and H. Shekaari, p-Phenylenediaminium iodide capping agent enabled self-healing perovskite solar cell, *Sci. Rep.*, 2020, **10**(1), 20011.

19 X.-Z. Zhu, *et al.*, 2D Perovskite Capping Layer Enabling Stable Perovskite Photovoltaics, *Sol. RRL*, 2024, **8**(8), 2301082.

20 M. A. Mahmud, *et al.*, In Situ Formation of Mixed-Dimensional Surface Passivation Layers in Perovskite Solar Cells with Dual-Isomer Alkylammonium Cations, *Small*, 2020, **16**(49), 2005022.

21 X. Zhao, *et al.*, Effect of steric hindrance of butylammonium iodide as interface modification materials on the

performance of perovskite solar cells, *Sol. RRL*, 2022, **6**(7), 2200078.

22 X. Jiang, *et al.*, Deeper insight into the role of organic ammonium cations in reducing surface defects of the perovskite film, *Angew. Chem., Int. Ed.*, 2022, **61**(12), e202115663.

23 H. Kim, *et al.*, Optimal Interfacial Engineering with Different Length of Alkylammonium Halide for Efficient and Stable Perovskite Solar Cells, *Adv. Energy Mater.*, 2019, **9**(47), 1902740.

24 K. Li, *et al.*, High Efficiency Perovskite Solar Cells Employing Quasi-2D Ruddlesden-Popper/Dion-Jacobson Heterojunctions, *Adv. Funct. Mater.*, 2022, **32**(21), 2200024.

25 T. R. Rana, *et al.*, Scalable Passivation Strategies to Improve Efficiency of Slot Die-Coated Perovskite Solar Cells, *ACS Energy Lett.*, 2024, **9**(4), 1888–1894.

26 Q. Lou, *et al.*, Room Temperature Ionic Liquid Capping Layer for High Efficiency FAPbI3 Perovskite Solar Cells with Long-Term Stability, *Adv. Sci.*, 2024, **11**(19), 2400117.

27 W. Yang, *et al.*, Visualizing Interfacial Energy Offset and Defects in Efficient 2D/3D Heterojunction Perovskite Solar Cells and Modules, *Adv. Mater.*, 2023, **35**(35), 2302071.

28 Y. Du, *et al.*, Manipulating the Formation of 2D/3D Heterostructure in Stable High-Performance Printable CsPbI3 Perovskite Solar Cells, *Adv. Mater.*, 2023, **35**(5), 2206451.

29 C. Zhang, *et al.*, Constructing a stable and efficient buried heterojunction *via* halogen bonding for inverted perovskite solar cells, *Adv. Energy Mater.*, 2023, **13**(2), 2203250.

30 S. Wu, *et al.*, Modulation of Defects and Interfaces through Alkylammonium Interlayer for Efficient Inverted Perovskite Solar Cells, *Joule*, 2020, **4**(6), 1248–1262.

31 C.-H. Tien, W.-S. Lai and L.-C. Chen, Buried Interface Passivation Using Organic Ammonium Salts for Efficient Inverted CsMAFA Perovskite Solar Cell Performance, *ACS Omega*, 2024, **9**(21), 23033–23039.

32 X. Wang, *et al.*, Interfacial Modification *via* a 1,4-Butanediamine-Based 2D Capping Layer for Perovskite Solar Cells with Enhanced Stability and Efficiency, *ACS Appl. Mater. Interfaces*, 2022, **14**(20), 22879–22888.